J Electroceram (2007) 18:347–353
DOI 10.1007/s10832-007-9186-3

Dielectric and pyroelectric anisotropy in the melt-quenched barium bismuth niobate ceramics

C. Karthik · K. B. R. Varma

Received: 28 December 2005 / Accepted: 20 June 2007 / Published online: 17 July 2007

Abstract $BaBi_2Nb_2O_9$ textured ceramics were fabricated via melt-quenching followed by high temperature (800–1000 °C) sintering process. The resulting ceramics possessed a {00l} texture with the a–b plane of the grains oriented parallel to the major face of the quenched plate. The influence of the sintering temperature on the orientation factor (f) and microstructure was evaluated via X-ray powder diffraction (XRD) and Scanning electron microscopy (SEM). The orientation factor was found to increase with increase in the sintering temperature and reached a maximum value of 0.47 for the samples sintered at 1000 °C for 10 h. Relative density and the grain-size of the ceramics were found to increase with increase in the sintering temperatures. The effect of texture on the dielectric and pyroelectric properties was evaluated. The measurements performed along the direction perpendicular to the pressing axis exhibited superior values than that of the direction parallel to the pressing axis. The observed anisotropy in the physical properties was attributed to the increased contribution from the highly polarizable a–b planes which are oriented in the direction perpendicular the pressing axis.

Keywords Aurivillius oxides · Relaxor ferroelectrics · Melt-quenching · Crystallographic texture

1 Introduction

Aurivillius family of ferroelectric oxides associated with a general chemical formula $Bi_2A_{n-1}B_nO_{3n+3}$ possess an anisotropic crystal structure containing alternate $[Bi_2O_2]^{2+}$ and n perovskite $[A_{n-1}B_nO_{3n+1}]^{2-}$ layers [1]. These materials have attracted much attention owing to their potential non-volatile random access memory (NVRAM) [2] and high temperature piezo-electric [3] applications. However the volatile nature of bismuth oxide makes the growth of stoichiometric single crystals of these materials very difficult and the randomly oriented ceramics show poor electrical properties. Further, the two dimensional nature of the ferroelectric switching makes the poling very difficult.

It was known that the physical properties of a ceramic could be enhanced by tailoring the microstructure, where the grain orientation is an important aspect. The textured or grain-oriented ceramics in which most grains are oriented in a particular crystallographic direction exhibit properties akin to that of single crystal [4]. The textured ceramics were known to exhibit superior properties in the direction of the polar axis. Grain orientation could be achieved through various techniques such as hot forging [5], hot pressing [6], cold pressing [7], melt-quenching [8] and templated grain growth (TGG) via tape casting [9–11]. TGG is the most widely used technique which involves orienting anisotropically shaped template particles via tape casting in a dense fine grained matrix. This method has been used to fabricate textured ceramics of several materials such as mullite [10], $Sr_{0.53}Ba_{0.47}Nb_2O_6$ [9], $Bi_4Ti_3O_{12}$ [12, 13] and $SrBi_2Ta_2O_9$ [14].

In this paper, we report the fabrication of {00l} textured $BaBi_2Nb_2O_9$ (BBN) by adopting a simple melt-quenching technique, which involves the melt-quenching of the reactants followed by sintering. Indeed, this method was widely used to fabricate textured ceramics of many Bi-based high temperature superconductors [8, 15]. BBN is an n=2 member of Aurivillius family of oxides associated

C. Karthik · K. B. R. Varma (✉)
Materials Research Centre, Indian Institute of Science, Bangalore, India
e-mail: kbrvarma@mrc.iisc.ernet.in

with relaxor characteristics [16–18]. To the best of the knowledge of the authors there are no details in the literature concerning the grain orientation of this class of relaxors, except a recent report on grain orientation of BBN via spark plasma sintering [19]. In the present study, the effect of sintering conditions on the grain orientation and microstructure was investigated. The dielectric and pyroelectric properties that were studied along two different directions which are parallel and perpendicular to the pressing axis were found to be anisotropic.

2 Experimental

The first step in the fabrication of textured BBN ceramics was the quenching of the melts of the constituent oxides. For this, the stoichiometric amount of constituent carbonates/oxides ($BaCO_3$, Bi_2O_3 and Nb_2O_5 (Aldrich chemicals)) were mixed well by using a pestle and mortar. Five weight percent extra amount of Bi_2O_3 was added to the initial mixture to compensate for the bismuth loss at high temperatures. The resultant mixture was packed into a platinum crucible and melted at 1100 °C using a Lenton glass melting furnace. The melt was held at this temperature for about 20 min and then it was poured over a stainless steel plate and pressed by another plate. The resultant product was a plate of about 4–5 mm thick. The phase analysis of the as-quenched plate was carried out using X-ray powder diffraction (XRD, Scintag USA) technique.

To achieve texture, the as-quenched samples were sintered at different temperatures ranging from 800 to 1000 °C for 10 h. The phase formation and the crystallographic texture of the sintered platy samples were examined by XRD. The degree of orientation ({00l} in the present case) was calculated using Lotgering's method, in which the orientation factor (f) was obtained using the formula,

$$f = \frac{(p - p_0)}{(1 - p_0)} \tag{1}$$

where $p = \Sigma I_{(001)} / \Sigma I_{(hkl)}$ for the textured sample and $p_o = \Sigma I_{(001)} / \Sigma I_{(hkl)}$ for the randomly oriented BBN powder prepared via the conventional solid state reaction route. ΣI_{00l} is the sum of X-ray intensity, reflected from {00l} family of planes and ΣI_{hkl} is the sum of reflected X-ray intensity from all the planes. The Scanning electron microscopy (SEM) (Cambridge Stereoscan S-360) was employed for the microstructural analysis of sintered ceramic plates. The densities of the samples were determined by Archimedes's method with Xylene (density, ρ= 0.87 g/cm^3) as the liquid media.

For electrical characterization, the sintered ceramics were cut and ground into two types of discs; one with the direction of measurement parallel (B| |) and the other in which, it is perpendicular (B⊥) to the pressing axis of the original quenched plate. For electroding, the polished surfaces were sputtered with gold and silver leads were bonded using silver epoxy. Capacitance measurements were carried out using a HP 4194A impedance–gain phase analyzer as a function of frequency (100 Hz to 1 MHz) and temperature (room temperature to 400 °C).

The direct method (Byer and Roundy) was used for pyroelectric current measurement. For this, the samples were poled under a field of about 3 kV/ cm at 150 °C prior to the measurements and the electrodes were short for about 30 min to eliminate the contribution arising from surface charges. The samples were then connected to a Keithley 485 auto ranging Picoammeter and the pyroelectric current was monitored as a function of temperature (room temperature to 400 °C) at a heating rate of 3 °C/min. The pyro electric coefficient 'p' was calculated using the relation,

$$p = \frac{I}{A(dT/dt)} \tag{2}$$

Where I is the pyroelectric current, A is the electrode area and dT/dt is the rate of heating.

3 Results and discussion

3.1 XRD and texture analyses

The XRD patterns recorded for the as-quenched and sintered BBN ceramic plates are depicted in Fig. 1(a–e).

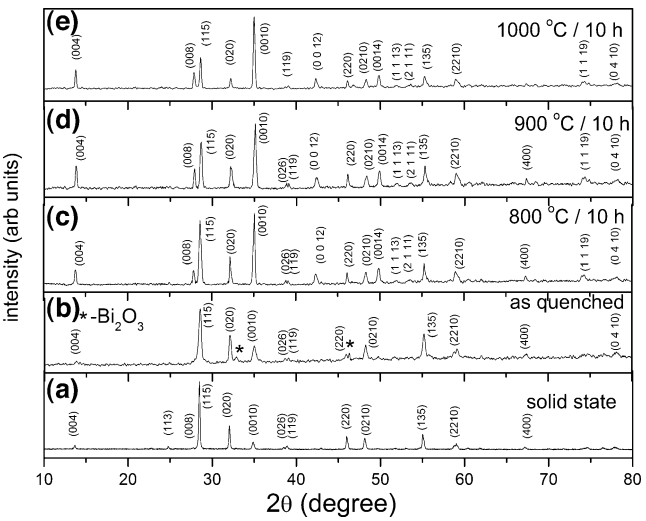

Fig. 1 XRD patterns of (**a**) BBN powder prepared via solid-state reaction route, (**b**) as-quenched BBN plate (**c–e**) quenched plate sintered at 800, 900 and 1000 °C for 10 h respectively

The XRD pattern of the BBN ceramic powder synthesized via conventional solid state reaction route is also shown Fig. 1(a) for comparison. The XRD pattern of the as-quenched sample [Fig. 1(b)] shows the presence of peaks corresponding to BBN layered perovskite. However, a few reflections corresponding to Bi_2O_3 were also identified. This shows that BBN ceramics can be prepared by a single step melt-quenching technique. The presence of unreacted Bi_2O_3 implies that the reaction for the formation of BBN was incomplete as the reaction time was short. The presence of rather broad peaks demonstrates the presence of fine grains in the as-quenched ceramics. Another interesting aspect is that the X-ray intensities of {00l} reflections are higher than that of a ceramic powder prepared via conventional solid state route. The Lotgering's factor ({00l} reflections) for the as-quenched ceramic was calculated to be around 0.12 implying that the crystallization of BBN takes place with the a–b plane parallel to the surface of the quenched plate during the process of quenching.

The XRD patterns of the samples sintered at 800, 900 and 1000 °C for 10 h are shown in Fig. 1(c–e). It is evident from these that the process of sintering leads to the crystallization of pure BBN and the reflections corresponding to Bi_2O_3 are absent. It is observed that the X-ray intensities of the {00l} planes of BBN dominate the XRD patterns of the sintered samples. The degree of {00l} texture increases with increase in sintering temperature. Figure 2 shows the variation of Lotgering's factor (f) calculated according to the XRD results as a function of sintering temperature. The value of '*f*' was found to increase from 0.32 for 800 °C/10 h sintered sample to 0.47 for 1000 °C/10 h sintered sample. This suggests that, during the process of sintering, the grain growth occurs in a preferential direction which is parallel to the plane of the ceramic plate and perpendicular to the pressing axis. The samples sintered at 1000 °C/10 h which showed the higher '*f*' value were selected for physical property studies.

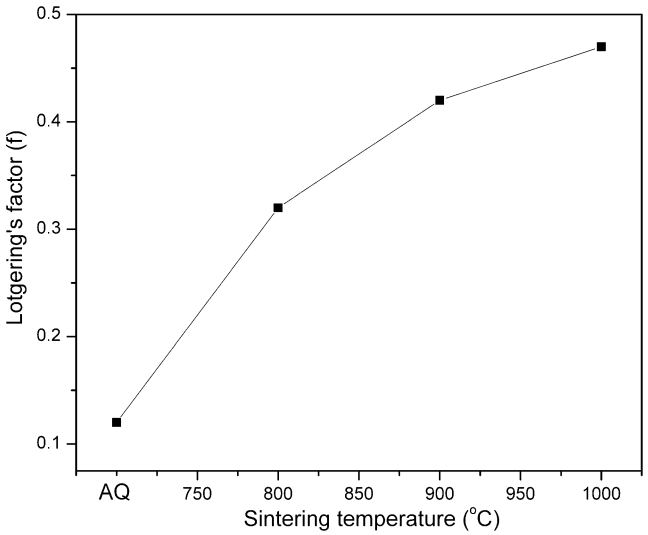

Fig. 2 Variation of Lotgering's factor (*f*) as a function of sintering temperature, where AQ denotes as-quenched sample

The above results indicate the development {00l} texture during the process of sintering. The mechanism responsible for this kind of texturing is not very clear as there is no temperature gradient across the sample during the process of sintering. Normally texturing is achieved with the aid of externally added template particles. In the present case, 47% orientation in the grains is accomplished in the absence of such particles. Therefore one plausible explanation could be that, during the process of quenching, the plate shaped crystallites which nucleate from the melt might get aligned parallel to the surface of the metal plates as the melt is squeezed in that direction. The alignment is such that the a–b plane of the crystallites is parallel to the major face of the quenched ceramic plate. Also there is a possibility for the two dimensional crystallization along the metal plate–melt interface during the process of pressing. These oriented crystallites of significant volume fraction would possibly act as template particles and facilitate the growth of oriented crystallites.

The texture development in the ceramics with preexisting template particles is a well established process. In the process of sintering, the coarsening of template particles occurs in which the matrix grains which are misaligned with the template particles form high energy boundaries and are easily consumed by the templates where as the grains oriented parallel to the templates form low-energy grain boundaries with the templates and are not consumed by the template particles. So effectively the volume fraction of the {00l} oriented grains increases at the expense of the disoriented grains.

The percentage of grain orientation achieved for BBN ceramics is comparable to that of the textured ceramics of other Aurivillius oxides fabricated via templated grain growth in which the template particles were synthesized separately and aligned via tape casting technique [14]. We believe that {00l} oriented grains that form while quenching serve as templates through out the sample. Indeed, the texture of the ceramics was confirmed at different depths from the surface by XRD studies after mechanical grinding.

3.2 Microscopic studies

Figure 3(a–c) shows the scanning electron micrographs recorded on the surface parallel to the plane of the plate for the samples sintered at 800, 900 and 1000 °C for 10 h respectively. Figure 3(d) depicts the cross-section of the sample sintered at 1000 °C for 10 h. It is clear from the Fig. 3(b–c) that most of the grains have a large flat area along the pressed plane. They are preferentially aligned

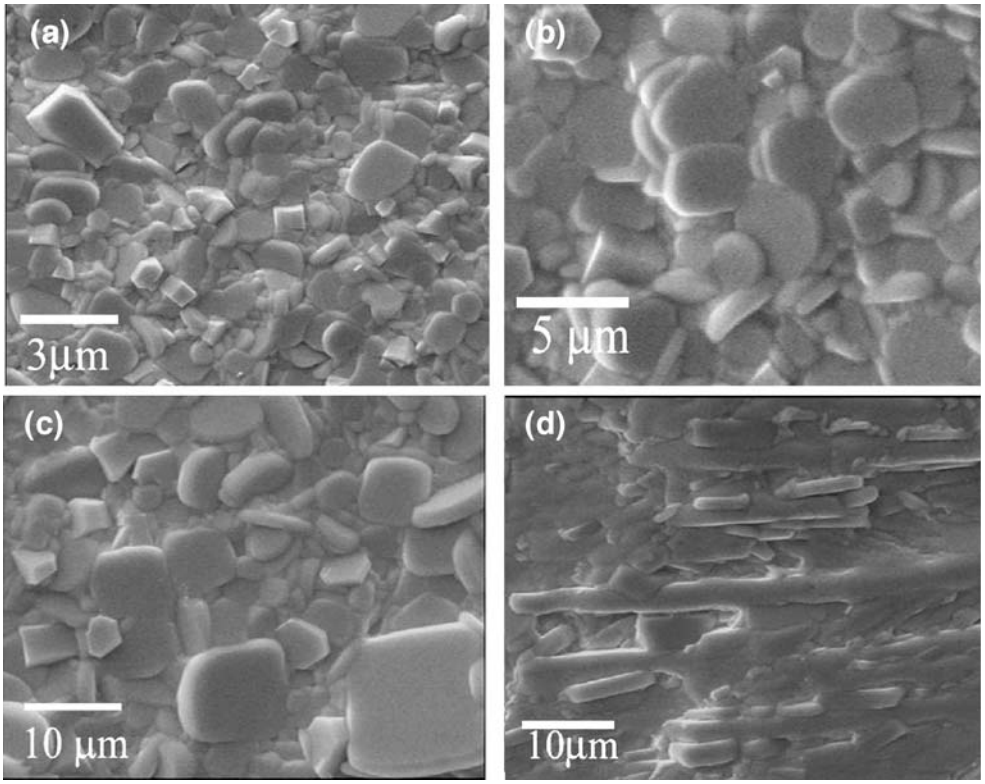

Fig. 3 Scanning electron micrographs of (**a–c**) Surfaces of the samples sintered at 800, 900 and 1000 °C for 10 h respectively and (**d**) cross-sectional view of the sample sintered at 1000 °C/10 h

along the plane perpendicular to the pressing direction and parallel to the surface of the quenched ceramic plate. The micrographs corresponding to the samples heat treated at 900 °C and 1000 °C show an increase in the size of the {00l} oriented grains and a decrease in the volume fraction of randomly oriented grains with increase in sintering temperature. This confirms the fact that the {00l} oriented grains grow at the expense of the randomly oriented grains. The micrograph corresponding to the cross-section of the sample sintered at 1000 °C/10 h depicted in Fig. 3(d) clearly demonstrates the alignment of the platy grains in a particular plane and these are observed to stack one above the other. The plates are characterized by a uniform thickness of about 1–2 μm and vary widely in the length ranging from few microns to several tens of microns. These results are consistent with those obtained by XRD analyses.

Figure 4 shows the variation of relative density as a function of sintering temperature. The as-quenched sample (AQ) showed a poor relative density of about 77%. Due to this, the as-quenched samples were mechanically not strong. The sintered samples showed improved density and it increases with increase in sintering temperature. The relative density of the sample sintered at 800 °C was about 88% and it reached a maximum value of about 95% for the sample sintered at 1000 °C. The increase in the relative density of the ceramics can be attributed to the elimination of porosity with the increase in sintering temperature. Also the contribution due to the evaporation of the secondary phase, bismuth oxide is not completely ruled out. The observed relative density is higher than that of the BBN ceramics sintered using the powders prepared via solid state reaction route where densities of only about 92–93% could be achieved. Interestingly the relative density is found to decrease with increase in the sintering temperature beyond 1000 °C which is attributed to the exaggerated grain growth accompanied by inter-granular pores.

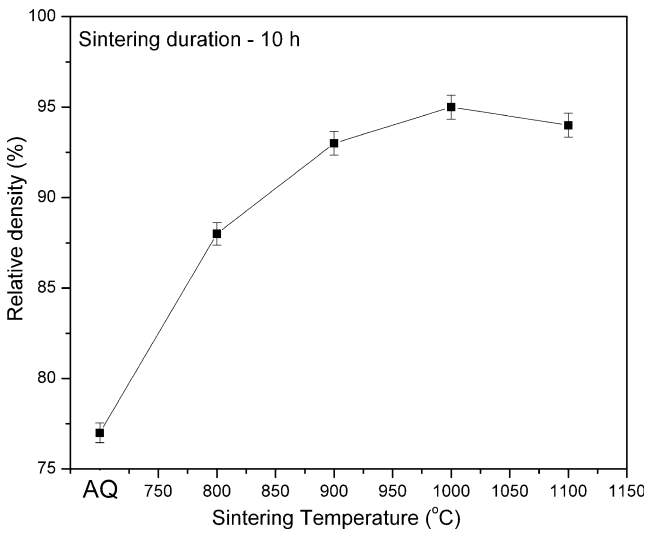

Fig. 4 Variation of relative density of BBN plates as a function of sintering temperature, where AQ denotes as-quenched sample

3.3 Dielectric studies

Figure 5(a–b) shows the temperature dependence of the dielectric constant (ε_r) and dielectric loss (D) measured at 100 kHz for the textured B| | and B⊥ samples sintered at 1000 °C for 10 h. Both the B| | and B⊥ samples exhibit the characteristic diffuse phase transition which is akin to that of the BBN ceramic fabricated via conventional route. Interestingly, a significant anisotropy in the dielectric constant was observed throughout the temperature range covered in the present studies. It is observed from Fig. 5(a) that the dielectric constant of the sample B⊥ (ε_r=305) is higher than the one obtained in the sample B| | (ε_r=286) at room temperature. The anisotropy in the dielectric constant is observed to be maximum (around 50) at the temperature of the dielectric constant maximum (T_m). The observed dielectric anisotropy is smaller that of the textured BBN ceramic prepared via spark plasma sintering [19], which may be because of the lesser degree of grain orientation in the present case. The observed loss depicted in Fig. 5(b) has almost the same value for both the orientations at low temperatures (<250 °C) and the loss in B⊥ sample increases more rapidly than the B| | one at high temperatures (>250 °C).

BBN was reported to be a relaxor ferroelectric with the characteristic frequency dependence of dielectric maximum. Shimakawa et al. [16] attributed the observed relaxor behavior to the polarization fluctuations in the nano polar regions that are present in the a–b plane of the perovskite blocks. In general, the displacement of B-site cations from its equilibrium position was considered to be the origin of ferroelectricity [1], but the subsequent studies showed that it is a complicated phenomenon with different structural factors contributing to it. According to Withers et al. [20], the three different contributions to spontaneous polarization are the displacement of A-site cations, the displacement of B-site cations and the averaged motion of oxygen ions within the bismuth oxide layer. However, the main structural cause of ferroelectricity was found to be the displacement of A-site cations along a-axis in the perovskite layer. The contribution from the c-axis or the plane perpendicular to the bismuth oxide layer is less significant. So the polar axis or the easy direction of polarization lies in the a–b planes in this class of compounds. Therefore, the observed anisotropy in ε_r is chiefly attributed to the grain orientation, where nearly half of the grains are oriented in such a way that the polar axes direction is parallel to the applied field in the samples that were cut perpendicular to the pressing axis. This explains in rationalizing the incidence of high ε_r in that direction.

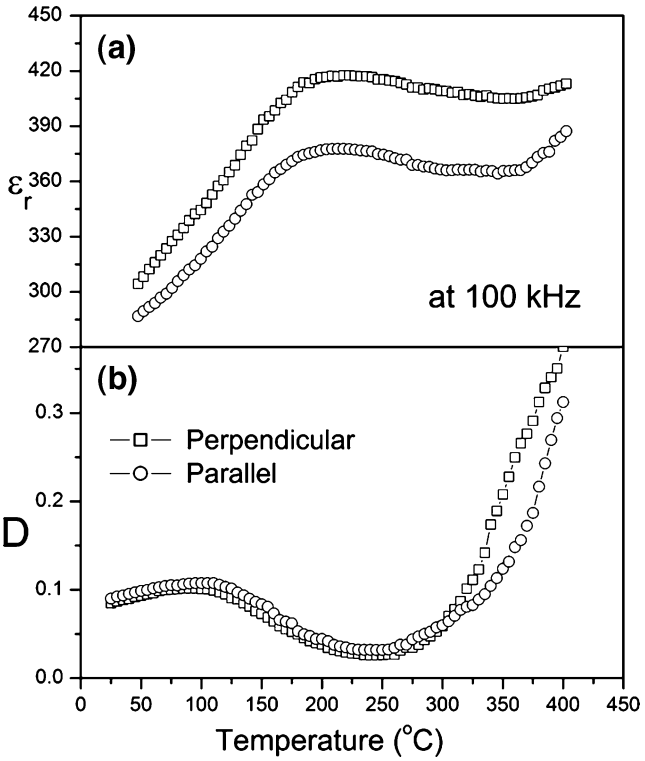

Fig. 5 Variation of (**a**) dielectric constant (ε_r) and (**b**) dielectric loss (D) as a function of temperature at 100 kHz for two different orientations

The observed high values of loss (D) at high temperatures in case of B⊥ samples as compared to that of B| | samples are attributed to the anisotropy in the conductivity. It is well known that the contribution to the ionic conductivity from the perovskite layer is higher than the bismuth oxide layer. This is because of the activation energy for oxygen ion migration in the bismuth oxide layer (>1.6 eV) is higher than the perovskite layer (~1 eV) [21]. The conductivity therefore can be considered to be dominant along the planes parallel to the bismuth oxide layers and this explains the higher values of dielectric loss in case of B⊥ samples where the bismuth oxide layer is parallel to the applied field.

The effect of crystallographic texture on the diffuseness in the phase transition has been studied by estimating the degree of diffuseness (γ) using the following relation,

$$(1/\varepsilon_r) = (1/\varepsilon_m) + (C)^{-1}(T - T_m)^{\gamma} \quad (3)$$

Where ε_m is the maximum value of the dielectric constant at the transition temperature (T_m), C is the Curie-like constant and γ is the degree of diffuseness. The limiting values 1 and 2 for γ respectively reduce the expression to the Curie–Weiss law valid for a normal and the quadratic dependence valid for the ideal relaxor ferroelectric. The slope of the log ($1/\varepsilon_r - 1/\varepsilon_m$) and log ($T - T_m$) plot gives the value of γ. Figure 6 shows the typical plots obtained for both the B| | and B⊥ samples. The value of the degree of diffuseness for B⊥ sample is 1.82 where as it is 1.72 for the B| | sample. This shows that the B⊥ sample behaves more

like an ideal relaxor than the B| | one, because of the increased contribution from the polar regions.

3.4 Anisotropy in pyroelectric coefficient

The effect of texturing on the polar nature of the ceramics can be directly visualized via the pyroelectric current measurements. Figure 7 shows the variation of pyroelectric coefficient (p) as a function of temperature for both the B| | and B⊥ samples. The pyroelectric coefficient increases with increase in temperature for both the samples and exhibits an anomaly around 225 °C which is consistent with the relaxor to paraelectric transition temperature (T_m) of the BBN ceramics. The room temperature value of the pyroelectric coefficient for B⊥ sample (7 nC cm^{-2} °C^{-1}) is higher than that of B| | sample (4 nC cm^{-2} °C^{-1}). The observed anisotropy is well pronounced in the vicinity of relaxor to paraelectric transition where the values of the pyroelectric coefficients for B| | and B⊥ samples are 0.085 μC cm^{-2} °C^{-1} and 0.5 μCcm^{-2} °C^{-1} respectively.

The pyroelectric coefficients are positive in the entire range of the temperatures under study for both the ceramics. In general the pyroelectric coefficient measured consists of two components, the primary effect arises because of the change in spontaneous polarization (P_s) and the secondary effect is piezoelectric in origin. In many ferroelectric oxides, the secondary effect was found to dominate which leads to the positive values of pyroelectric coefficients. For instance, the textured ceramics of $Sr_xBa_{1-x}Nb_2O_6$ was found to show high positive values of pyroelectric coefficients [9, 22].

Apart from these effects, the presence of space charges and surface charges may significantly contribute to the bulk polarization of the ceramic especially when there is a finite electrical conductivity associated with the ceramics. In the case of relaxor ceramics with finite electrical conductivity, the pyroelectric current has a complex character and was found to exhibit a broad anomaly in the temperature region of relaxor to paraelectric transition [23]. Recently Adamczyk et al. [17] has reported the thermally induced depolarization current (TSDC) measurements of $BaBai_2Nb_2O_9$ ceramics in which the poling conditions were similar as that of the present study and an anomaly in the TSDC current was observed at the same temperature region as that of the present case. The observed anomaly was attributed to the mutual interaction of the orientation part of the metastable polarization and the polarization of the free ion and electron space charges, participating in the screening process of the polar regions. The pyroelectric behavior and the anomaly observed for the textured BBN in the present study can also be attributed to the same reasons. It is interesting to note the anisotropy in the values of pyroelectric coefficients measured in two directions, which can be attributed to different reasons such as the high polarizability as well as high conductivity in case of B⊥ samples. The conductivity contribution to the observed pyroelectric behavior is seemed to be significant, so the anisotropy in the conductivity would have a prominent effect on the pyroelectricity making it anisotropic.

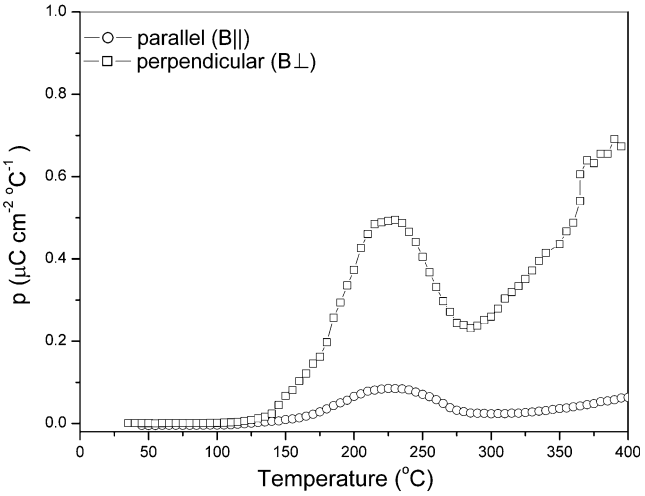

Fig. 7 Variation of pyroelectric co-efficient (p) as a function of temperature for two different orientations

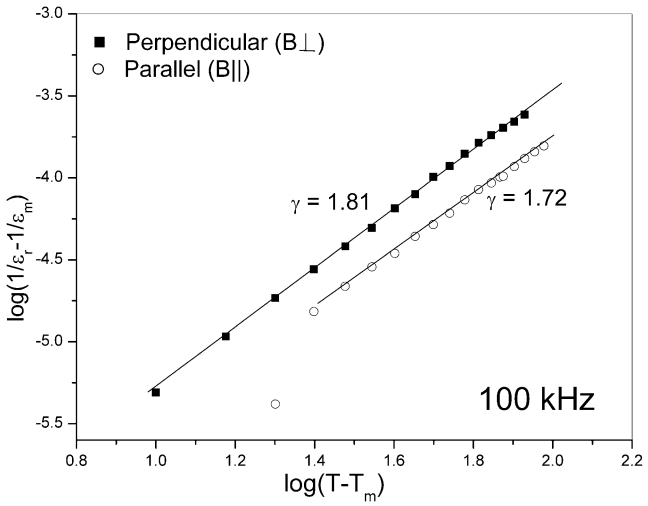

Fig. 6 Variation of log ($1/\varepsilon_r - 1/\varepsilon_m$) with log ($T - T_m$) for two different orientations

4 Conclusions

Significant anisotropy in both the dielectric constant and the pyroelectric coefficients were encountered in the BBN ceramics prepared by conventional melt-quenching followed by heat treatment. The anisotropy especially in the pyroelectric coefficient is appreciably high in the vicinity of relaxor to paraelectric transition temperature. The dielectric

and pyroelectric properties were found to have superior values in the direction perpendicular to the quenching axis. These are attributed to the partial grain orientation that is achieved which in turn enhances the contribution from the polar a–b plane.

Acknowledgements The authors thank the Department of Science and Technology (DST), Government of India for the financial support.

References

1. R.E. Newnham, R.W. Wolfe, J.F. Dorrian, Mater. Res. Bull. **6** (1971)
2. W.L. Warren, B.A. Tuttle, D. Dimos, Appl. Phys. Lett. **67**, 1426 (1995)
3. D. Damjanovic, Curr. Opin. Solid State Mater. Sci. **3**, 469 (1998)
4. T. Takenaka, K. Sakata, Jpn. J. Appl. Phys. **19**, 31 (1980)
5. M. Venet, A. Vendramini, I.A. Santos, J.A. Eiras, D. Garcia, Mater. Sci. Eng. B **117**, 254 (2005)
6. J. Rodel, A.M. Glaeser, J. Am. Ceram. Soc. **73**, 3292 (1990)
7. K. Shantha, K.B.R. Varma, Mater. Res. Bull. **32**, 1581 (1997)
8. S.J. Peng, M.D. Lan, P. Klavins, J.Z. Liu, R.N. Shelton, Physica C **212**, 301 (1993)
9. C. Duran, S. Trolier-Mckinstry, G.L. Mesing, J. Am. Ceram. Soc. **83**, 2203 (2000)
10. I.E. Gonenli, G.L. Messing, J. Eur. Ceram. Soc. **21**, 2495 (2001)
11. Y. Kan, P. Wang, Y. Li, Y.-B. Cheng, D. Yan, J. Eur. Ceram. Soc. **23**, 2163 (2003)
12. J.L. Jones, S.C. Vogel, E.B. Slamovich, K.J. Boman, Scr. Mater. **51**, 1123 (2004)
13. J.A. Horn, S.C. Zhang, G.L. Messing, S.T-Mckinstry, J. Am. Ceram. Soc. **82**, 921 (1999)
14. H. Amorin, A.L. Kholkin, M.E.V. Costa, J. Eur. Ceram. Soc. **25**, 2453 (2005)
15. I. Monot, M.P. Delamare, J. Wang, G. Desgardin, B. Raveau, Physica C **235**, 457 (1994)
16. Y. Shimakawa, Y. Kubo, Y. Nakagawa, S. Goto, T. Kamiyama, H. Asano, F. Izumi, Phys. Rev. B **61**, 6559 (2000)
17. M. Adamczyk, Z. Ujma, M. Pawelczyk, J. Mater. Sci. **41**, 5317 (2006)
18. A.L. Kholkin, M. Avdeev, M.E.V. Costa, J.L. Bapista, S.N. Dorogovtsev, Appl. Phys. Lett. **79**, 662 (2001)
19. H. Yan, H. Zhang, R. Ubic, M. Reece, J. Liu, Z. Shen, J. Mater. Sci., Mater. Electron. **17**, 657 (2006)
20. R.L. Withers, J.G. Thompson, A.D. Rae, J. Solid State Chem. **94**, 404 (1991)
21. M.S. Islam, S. Lazure, R.N. Vannier, G. Nowogrochi, G. Mairesse, J. Mater. Chem. **8**, 655 (1998)
22. M. Venet, I.A. Santos, J.A. Eiras, D. Garcia, Solid State Ion. **177**, 589 (2006)
23. Z. Ujma, M. Adamczyk, J. Handerek, J. Eur. Ceram. Soc. **18**, 2201 (1998)